

## CLIMATOLOGY

# Climate change increases risk of extreme rainfall following wildfire in the western United States

Danielle Touma<sup>1,2\*</sup>, Samantha Stevenson<sup>1</sup>, Daniel L. Swain<sup>3,4,5</sup>, Deepti Singh<sup>6</sup>, Dmitri A. Kalashnikov<sup>6</sup>, Xingying Huang<sup>1,2</sup>

Post-wildfire extreme rainfall events can have destructive impacts in the western United States. Using two climate model large ensembles, we assess the future risk of extreme fire weather events being followed by extreme rainfall in this region. By mid-21st century, in a high warming scenario (RCP8.5), we report large increases in the number of extreme fire weather events followed within 1 year by at least one extreme rainfall event. By 2100, the frequency of these compound events increases by 100% in California and 700% in the Pacific Northwest in the Community Earth System Model v1 Large Ensemble. We further project that more than 90% of extreme fire weather events in California, Colorado, and the Pacific Northwest will be followed by at least three spatially collocated extreme rainfall events within five years. Our results point to a future with substantially increased post-fire hydrologic risks across much of the western United States.

## INTRODUCTION

Recently burned areas have an elevated risk of debris flows, mudslides, and flash floods during rain events due to wildfire-induced changes in soil properties, vegetation loss, and ground cover (1–5). These events are often sudden and difficult to predict—and can sometimes be deadly and destructive in populated areas. Hydrologically relevant effects within fire footprints can linger for up to a decade—incurring the risk of debris flows for up to 3 to 5 years following fire as the ground cover and fine roots recover, and the risk of flash floods for up to 5 to 8 years following fire as the soil returns to normal absorbance and vegetation regrowth (2). Meanwhile, more severe regional impacts can occur when extreme rainfall occurs within 1 or 2 years after a wildfire (1, 6), compounding the consequences of each and resulting in a higher impact event, especially if recovery efforts from the previous wildfire are still ongoing (7, 8).

The western United States is particularly vulnerable to the combined effects of wildfire and extreme rainfall, experiencing both hazards on a consistent basis. As a recent case, debris flows in Glenwood Canyon, Colorado in July 2021 occurred following heavy rainfall over the areas burned by the Grizzly Creek Fire in the previous year. These debris flows led to severe damages to infrastructure and roadways, shutting down a vital east-to-west connector across the Rocky Mountains. Post-fire rainfall events within shorter time frames have also had deadly consequences: In January 2018, Montecito in southern California experienced debris flows after a short but intense storm occurred over the footprint of the December 2017 Thomas Fire, leading to 23 fatalities and \$200 million in property damage (3). Farther north, in Okanogan County, Washington, a severe summer storm in 2014 caused mudslides and flash floods within the 1-month-old

Carlton Complex Fire footprint, destroying homes and blocking major highways (4). Understanding the risk of these linked events in a changing climate is therefore crucial for informed emergency management and community adaptation.

Previous research suggests that extreme wildfires are likely to increase in both frequency and intensity in the western United States in response to anthropogenic climate change. Fire intensity and area burned are expected to increase under expanding and intensifying drought conditions (9, 10), which favor the development of extreme fire weather conditions (11–13), continued fire suppression and exclusion (14, 15), and population increases in the wildland-urban interface (16, 17) in the 21st century (18). In addition, extreme fire weather conditions are expected to occur over a longer fire season in many regions (11), resulting in a shorter gap between the fire season and the wet season in places such as California (19). By mid-21st century, a “new normal” of heightened fire weather conditions are expected under projected warming (12, 20).

Simultaneously, significant increases in the magnitude and frequency of extreme precipitation are projected for the early 21st century in much of the western United States (21), and by mid-century, the frequency and rainfall volume of mid-sized heavy precipitation events are expected to increase by more than 30% (22). These effects are particularly pronounced in California: During the most extreme atmospheric river-driven events, California is projected to receive ~25% more precipitation—with maximum precipitation rates during these events potentially increasing by 50% or more in some areas (23), along with an increasing fraction of precipitation falling as rain rather than snow (24). Extreme wet and dry years in California are also expected to alternate more rapidly in a warming climate, likely increasing the odds of extreme precipitation events occurring within 1 or 2 years after a wildfire (25), and the severity of same-year sequential burned area-extreme precipitation events is expected to increase (26).

Since robust increases are expected for both wildfire and extreme rainfall events individually, the risk of these events occurring close together in time would also be expected to increase. However, to date, it has been difficult to quantify the impact of both anthropogenic climate change and climate variability on compounding extremes

Copyright © 2022  
The Authors, some  
rights reserved;  
exclusive licensee  
American Association  
for the Advancement  
of Science. No claim to  
original U.S. Government  
Works. Distributed  
under a Creative  
Commons Attribution  
NonCommercial  
License 4.0 (CC BY-NC).

Downloaded from <https://www.science.org> on October 07, 2022

<sup>1</sup>Bren School of Environmental Science and Management, University of California, Santa Barbara, Santa Barbara, CA, USA. <sup>2</sup>Climate and Global Dynamics Lab, National Center for Atmospheric Research, Boulder, CO, USA. <sup>3</sup>Institute of the Environment and Sustainability, University of California, Los Angeles, Los Angeles, CA, USA. <sup>4</sup>Capacity Center for Climate and Weather Extremes, National Center for Atmospheric Research, Boulder, CO, USA. <sup>5</sup>The Nature Conservancy of California, San Francisco, CA, USA. <sup>6</sup>School of the Environment, Washington State University, Vancouver, WA, USA.

\*Corresponding author. Email: [detouma@ucar.edu](mailto:detouma@ucar.edu)

such as these due to their rarity in both the relatively short observational record and in climate model simulations with small ensemble sizes (27). To quantify these limitations, we compare two initial-condition large ensemble simulations [Community Earth System Model v1 Large Ensemble (CESM1-LE) and Canadian Earth System Model v2 (CanESM2)] (28) to assess the changes in the frequency and likelihood of temporally compounding extreme fire weather and extreme rainfall events over the 21st century in the western United States. Because of their size (40 and 50 members each, respectively), these global large ensemble simulations raise the prospect of providing more robust statistics regarding rare events in a warming climate and allow investigation of changes to high-frequency (daily to annual) events on decadal to multidecadal time scales. The bulk of our analysis is focused on CESM1-LE (29), which has sufficient fire weather and rainfall data available and has substantially higher spatial resolution than CanESM2. We assess changes in events that are temporally compounding on subannual to multiannual time scales, capturing a range of hydrologic risk and impacts.

## RESULTS

### Future increasing frequency of extreme fire weather events

To capture daily meteorological conditions that shape wildfire risk, we use a modified version of the Canadian Forest Fire Weather Index (FWI), calculated using daily maximum temperature, precipitation, relative humidity, and surface wind speed (30–32). We calculate FWI for CESM1-LE and CanESM2 ensemble simulations from the Multi-Model Large Ensemble Archive (MMLEA) (28), which has sufficient data to calculate FWI (see Materials and Methods and table S1). At each grid cell, the 99.9th percentile of FWI, calculated using the 1980–2005 daily distribution of the pooled ensemble members of each large ensemble experiment, is used to identify extreme fire weather events ( $FWI_{99.9}$ ), capturing days during which ignited fires are likely to spread. While FWI does not account for vegetation characteristics or ignitions, extreme levels of FWI have been shown to correspond strongly with large burned areas over the western United States in observations (11, 20, 33) and have been reliably estimated using climate model simulations [e.g., (12)].

We quantify projected future changes in  $FWI_{99.9}$  frequency under the Representative Concentration Pathway (RCP8.5) scenario over the course of the 21st century and find more than a twofold increase in the Pacific Northwest (PNW) and eastern Colorado in both CESM1-LE (Figs. 1, A to C, 2, and 3A) and CanESM2 (figs. S1 and S2A). In addition, CESM1-LE shows large and significant ( $P < 0.05$ ) increases over most of California, with  $FWI_{99.9}$  becoming at least 100% more frequent by 2040 and 200% more frequent by 2100 (Fig. 1, A to C). However, CanESM2 shows small or insignificant changes in  $FWI_{99.9}$  frequency over this same region (Figs. 1 and 3A versus figs. S1 and S2A). We note that the magnitude of historical (pre-2005)  $FWI_{99.9}$  annual frequency is larger in CESM1-LE ( $\sim 2$  per  $10^5$  km<sup>2</sup>) than in CanESM2 ( $\sim 0.5$  per  $10^5$  km<sup>2</sup>) for all regions (Fig. 3A and fig. S2A). This may be due to the number of grid points per the area considered ( $FWI_{99.9}$  events are considered on the grid-point level), as well as the sequencing of days that exceed the 99.9th percentile of FWI (consecutive days are considered as one  $FWI_{99.9}$  event).

The differences in projections of  $FWI_{99.9}$  events between CESM1-LE and CanESM2 may be attributed to their disagreement on the magnitude of temperature change under RCP8.5, previously documented over this region (34). Given that warming temperatures are a prominent

driver of increases in extreme fire weather frequency in future projections, the uncertainty in projected warming is likely contributing to the uncertainty in extreme fire weather projections (12, 20). Moreover, a considerable portion of this uncertainty may stem from the large differences in the spatial resolution between CanESM2 ( $\sim 2.8^\circ \times 2.8^\circ$ ) and CESM1-LE ( $\sim 1.3^\circ \times 0.9^\circ$ ), and hence the representation of topography critical to the representation of fire weather variables such as wind speed and relative humidity at the surface [e.g., (33)]. Nonetheless, it is difficult to further understand the role of model uncertainty in the discrepancies in projections of  $FWI_{99.9}$  frequency under climate change and climate variability without additional large ensemble simulations with FWI data availability, especially ensembles with spatial resolution similar to or finer than that of CESM1.

The higher resolution of CESM1-LE, and therefore greater number of total grid points over the western United States, allows us to discern geographical heterogeneity in the projected response. We find that inland regions of California and PNW show robust (here defined as greater than two-thirds agreement across the ensemble members) and significant increases in  $FWI_{99.9}$  frequency during the early 21st century, while the immediate coastal areas show little or no robust increases by the end of the 21st century (Fig. 1, A to C). The lack of changes in  $FWI_{99.9}$  over these regions may be due to the poorly resolved coastal topography relevant to fire-fueling katabatic winds (35).

### Future increasing frequency of extreme rainfall events

Next, we consider changes to extreme rainfall frequency over the 21st century under RCP8.5 for CESM1-LE and CanESM2, and three additional large ensemble simulations that have sufficient daily precipitation data [CSIRO-Mk3.6, EC-Earth, and Geophysical Fluid Dynamics Laboratory's Coupled Model version 3 (GFDL-CM3); table S1]. Similar to our definition of extreme fire weather, we use exceedances above the 99.9th percentile of daily rainfall to identify extreme rainfall events ( $R_{99.9}$ ), which has been shown to often yield high-impact events in the observational record [e.g., (36)].

In the early part of the 21st century, robust increases in  $R_{99.9}$  frequency over a diagonal axis extending from the eastern PNW to western Colorado are seen for all models, consistent with recent studies [e.g., (37, 38)]. On the other hand, many models show that there are smaller or nonrobust increases in the coastal regions of California and PNW, as well as east of the Rocky Mountains (Figs. 1D and 3B and figs. S2B, S3, and S4). The lack of changes may be due to the insufficient complexity in the representation of topography in these relatively low-resolution models that are needed to simulate the precipitation amounts observed during extreme precipitation events [e.g., (39)]. In the mid-21st century (2041–2070), more regions begin to show significant increases in  $R_{99.9}$  frequency in the large ensemble simulations, and by 2100, most of the study domain shows robust increases in  $R_{99.9}$  frequency across the simulations (Fig. 1, D to F, 2, and 3B, and figs. S3 and S4). We note that there are differences between models in the absolute  $R_{99.9}$  frequency (Fig. 3B and fig. S4). This is likely attributable due to uncertainties in changes to atmospheric circulation over the western United States among the models, as well as differences in their temperature projections, which could drive further uncertainties regarding the magnitude of the thermodynamic response of rainfall (37, 38, 40).

### Temporally compounding events occurring within 1 year

Given that the spatial patterns and timing of changes under RCP8.5 differ substantially between the frequencies of  $FWI_{99.9}$  and  $R_{99.9}$

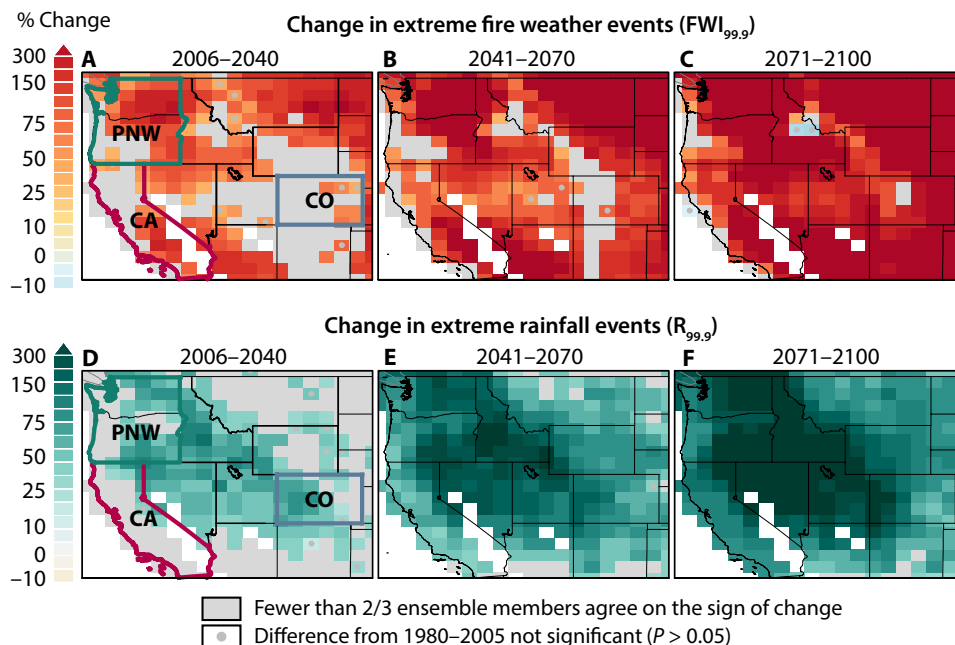


**Fig. 1. Change in the annual frequency of extreme fire weather ( $FWI_{99.9}$ ) and extreme rainfall ( $R_{99.9}$ ) events using CESM1-LE.** Ensemble mean percent change in annual frequency of  $FWI_{99.9}$  (A and C) and  $R_{99.9}$  (D to F) in 2006–2040 (A and D), 2041–2070 (B and E), and 2071–2100 (C and F) relative to the historic (1980–2005) frequency. Consecutive days that exceed the  $FWI_{99.9}$  threshold are considered as one event, dated on the first consecutive day. Gray areas are locations where fewer than two-thirds of the ensemble members agree on the sign of change, and gray stippling shows locations that do not have significant ( $P > 0.05$ ) differences in the ensemble distribution of frequency compared to 1980–2005 calculated using the Kolmogorov-Smirnov (KS) test. If both cases are true, the grid box will be shaded gray. White areas are desert, ocean, or surface water. (Results for CanESM2, CSIRO-Mk3-6-0, EC-Earth, and GFDL-CM3 are shown in figs. S1 and S3.)

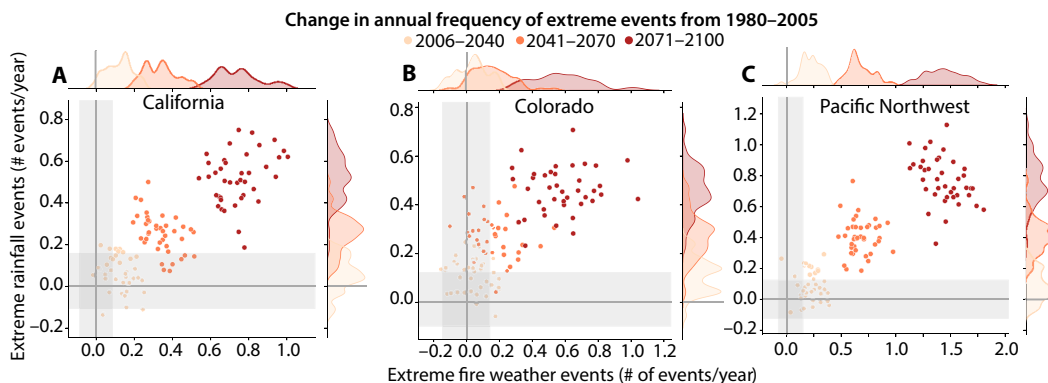


**Fig. 2. Joint frequency of extreme rainfall and extreme fire weather events using CESM1-LE.** Distributions of changes in the annual frequency of  $R_{99.9}$  (y axis) and  $FWI_{99.9}$  (x axis) events for 2006–2040, 2041–2070, and 2071–2100 for (A) California, (B) Colorado, and (C) PNW. Each data point indicates the change in an individual ensemble member. The gray horizontal and vertical bands show the minimum and maximum boundaries of the ensemble 1980–2005 variability. The regional annual frequency is calculated by averaging the frequency of  $R_{99.9}$  and  $FWI_{99.9}$  over all grid points in the region for each year and each ensemble member. Consecutive days that exceed the  $FWI_{99.9}$  threshold are considered as one event, dated on the first consecutive day.

events, individually, it is key that we explore the changes in the sequencing of these extreme events. We quantify the changes in the frequency and fraction of  $FWI_{99.9}$  events that are followed by  $R_{99.9}$  events on “subannual” (3 months, 6 months, and 1 year) time frames for the CESM1-LE and CanESM2 ensembles. The compounding impacts of these events on short time scales pose elevated risks of flash floods and debris flows (2, 7, 41).

Between 1980 and 2005, approximately one-third of  $FWI_{99.9}$  events are followed by  $R_{99.9}$  events within the first year over the

western United States in the CESM1-LE and CanESM2 ensembles, which is approximately  $\sim 1$  annual event per  $10^5 \text{ km}^2$  for CESM1-LE (Fig. 3, C and E, and figs. S5, E and F, and S6I). Under the RCP8.5 future warming scenario, we find robust increases in the fraction and number of  $FWI_{99.9}$  events that are followed by  $R_{99.9}$  events, as well as the number of  $R_{99.9}$  events that follow  $FWI_{99.9}$  events within subannual time frames. In CESM1-LE, western Colorado and most of the PNW see significant ( $P < 0.05$ ) increases in the fraction and number of  $FWI_{99.9}$  events followed by  $R_{99.9}$  events within 3 months,

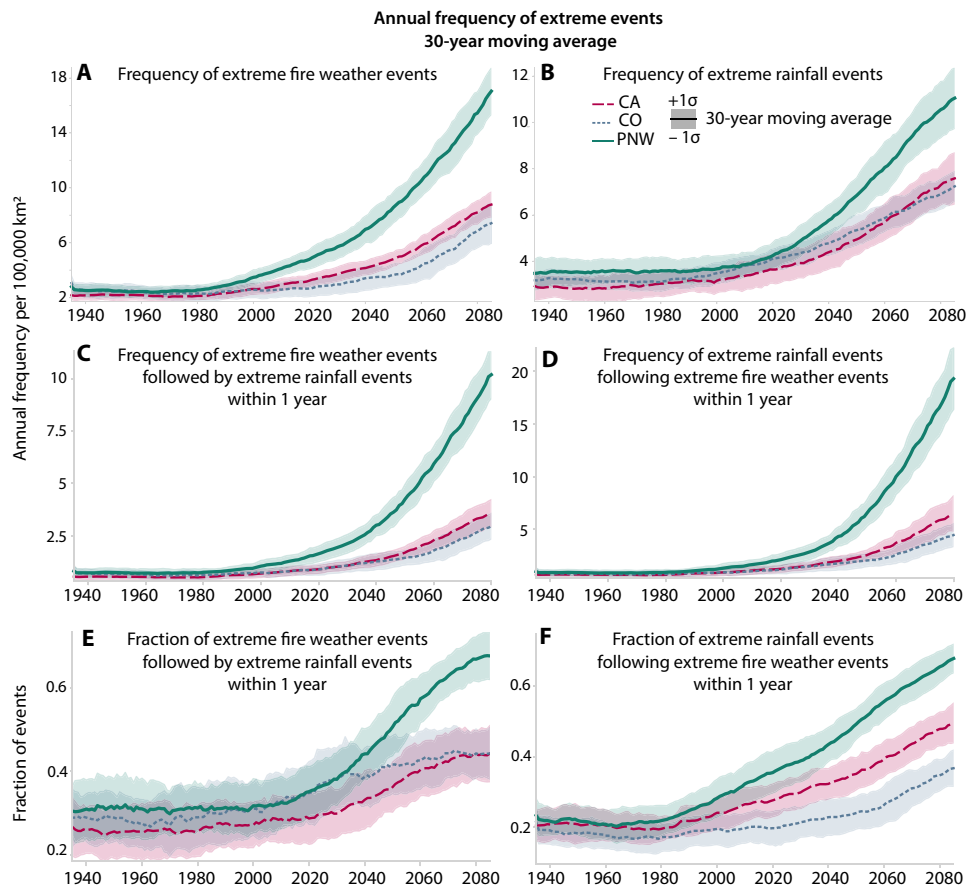


**Fig. 3. Historical and future frequency of extreme rainfall, extreme fire weather, and temporally compounding events using CESM1-LE.** Thirty-year moving average of annual frequency per  $10^5$  km<sup>2</sup> of (A) extreme fire weather (FWI<sub>99,9</sub>) events, (B) extreme rainfall events ( $R_{99,9}$ ), (C) FWI<sub>99,9</sub> events that are followed by  $R_{99,9}$  within 1 year, and (D)  $R_{99,9}$  events that follow FWI<sub>99,9</sub> events within 1 year from 1935 to 2085 for California (red dashed line), Colorado (blue dotted line), and the PNW (green solid line). (E) The fraction of FWI<sub>99,9</sub> events that are followed by  $R_{99,9}$  events and (F) the fraction of  $R_{99,9}$  events for that occur 1 year after a FWI<sub>99,9</sub> event within 1 year from 1935 to 2085 for California, Colorado, and PNW. Regional averages are calculated for the region boundaries shown in Fig. 1 and normalized by the total area of the state—for reference, California is approximately 420,000 km<sup>2</sup>. The lines represent the ensemble mean, and the shading is  $\pm 1$  SD of the 30-year moving average ensemble spread. (Results for CanESM2, CSIRO-Mk3-6-0, EC-Earth, and GFDL-CM3 are shown in figs. S2 and S4.)

from ~0% and almost none per year in 1980 to 40% and 0.3 per year in 2100 (Figs. 4, A to C, and 5, A to C, and fig. S5, A and B). Increases in the frequency and fraction of FWI<sub>99,9</sub> events followed by  $R_{99,9}$  events over the PNW are also present in CanESM2, showing a robust response to RCP8.5 forcing among the two models (figs. S6, A to D, and S7, A to D). However, while CESM1-LE shows the presence and increase in FWI<sub>99,9</sub> events followed by  $R_{99,9}$  events within 3 months over Idaho, Utah, northern Nevada, and western Colorado throughout the 21st century, CanESM2 does not (Figs. 4, A to C, and 5, A to C, and figs. S5, A and B, S6, A to D, and S7, A to D), which could be partly attributed to the lack of significant changes in extreme fire weather events over these regions in CanESM2 (fig. S1, D to F). This highlights that projections of compound events occurring within a relatively small time frame, i.e., 3 months, could be relatively more sensitive to projections of extreme events individually.

Significant increases in the fraction and number of FWI<sub>99,9</sub> events followed by  $R_{99,9}$  events within 6 months or 1 year are more widespread and emerge earlier. By the end of the century, more than 50% of FWI<sub>99,9</sub> events are followed by  $R_{99,9}$  in parts of the PNW, Nevada, Idaho, and Utah in both CESM1-LE and CanESM2 (Fig. 4, D to I, and fig. S6, E to L). Over the PNW, this equates to ~10

annual events per  $10^5$  km<sup>2</sup> (Fig. 3C) in CESM1-LE. While relatively modest compared to the PNW, California and Colorado also see significant ( $P < 0.05$ ) increases in the fraction and number of FWI<sub>99,9</sub> events followed by  $R_{99,9}$  within 6 months and 1 year (Figs. 3, C to E, 4, F and I, and 5, F and I, and figs. S6, H and L, and S7, H and L). In CESM1-LE, these increases are especially notable in western Colorado and northern California, where two-thirds of FWI<sub>99,9</sub> events are projected to experience an  $R_{99,9}$  event within 1 year at the end of the 21st century, representing a twofold or more increase from the historic period.

These increases in FWI<sub>99,9</sub> events followed by  $R_{99,9}$  events over northern California are also large and robust in the CanESM2 simulations, despite showing small or statistically insignificant changes in extreme fire weather frequency, alone (fig. S1 versus fig. S6). In this case, increases in extreme rainfall events could largely be driving the increases in FWI<sub>99,9</sub> events followed by  $R_{99,9}$  events, with more extreme rainfall events occurring in locations where they are historically relatively rare. In addition, shifts in the seasonality of extreme fire weather events, not evident through changes in annual frequency alone, could also be driving increases in subannual compound events.

## Fraction of extreme fire weather events followed by extreme rainfall events

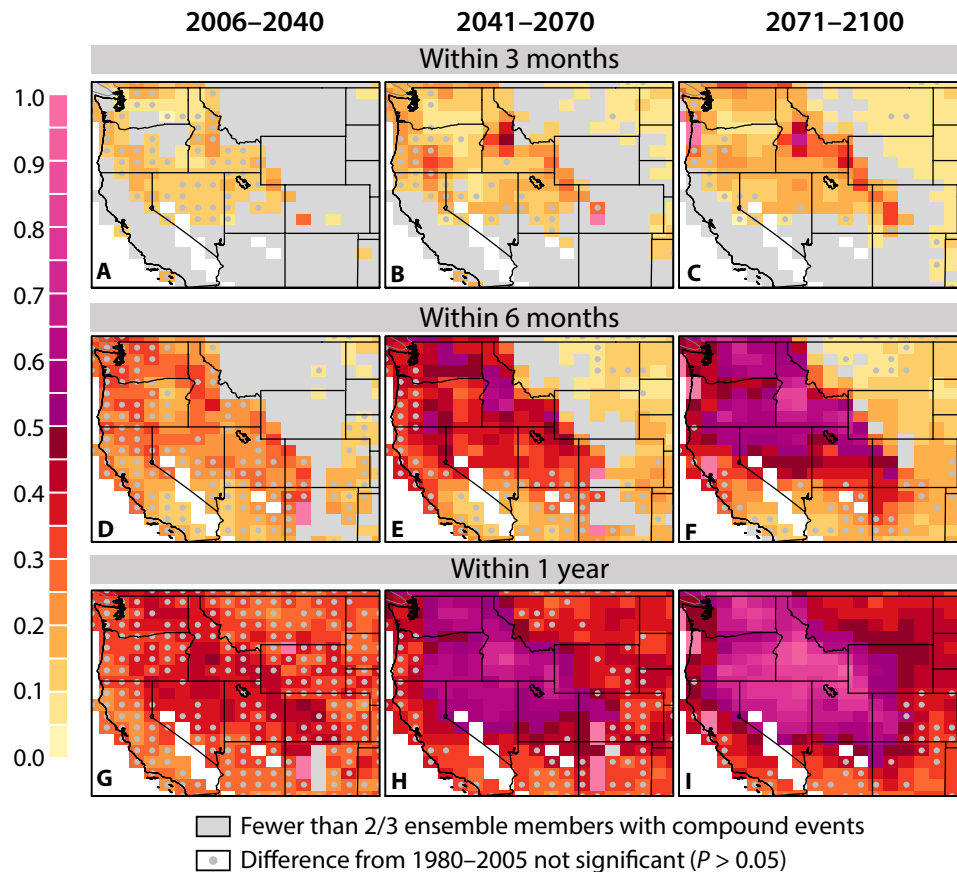


**Fig. 4.** If an extreme fire weather event occurs, what fraction are followed by extreme rainfall on subannual time frames using CESM1-LE? Fraction of extreme fire weather events ( $FWI_{99.9}$ ) followed by extreme rainfall events ( $R_{99.9}$ ) within (A to C) 3 months, (D to F) 6 months, and (G to I) 1 year in 2006–2040 (A, D, and G), 2041–2070 (B, E, and H), and 2071–2100 (C, F, and I). Consecutive days that exceed the  $FWI_{99.9}$  threshold are considered as one event, dated on the first consecutive day. Gray areas show where fewer than two-thirds of the ensemble members show at least one compound event occurring. Stippled regions do not have significant ( $P > 0.05$ ) differences in the ensemble distribution of likelihood compared to 1980–2005 (shown in fig. S5) calculated using the KS test. White areas are desert, ocean, or surface water. (Results for CanESM2 are shown in fig. S6.)

However, this is not the case in southern California for CanESM2, where strong increases in  $R_{99.9}$  events (fig. S3, D to F) are insufficient in producing significant increases in the number or fraction of  $FWI_{99.9}$  events followed by  $R_{99.9}$  events within 6 months or 1 year (figs. S6, E to L, and S7, E to L). In this region, the discrepancies in the projections of  $FWI_{99.9}$  frequency between CESM1-LE and CanESM2 alone are reflected in changes in compound events, where CESM1-LE shows statistically significant increases in 6-month and 1-year compounding events, while CanESM2 does not (Figs. 4, D to I, and 5, D to I, versus figs. S6, E to L, and S7, E to L). In this case, additional understanding of the discrepancies among the model projections of individual events could shed more light on the uncertainty of compound event projections. We again emphasize, however, that it is plausible that CanESM2 is simply not capable of representing the highly topography-dependent physical processes that drive extreme  $FWI_{99.9}$  events (i.e., Santa Ana wind and low-humidity events) in this region due to its much coarser spatial resolution compared to CESM1.

We further find that, at a subregional level of spatial aggregation, increases in the frequency of compound extreme fire weather-rainfall

events are the product of increases in both  $FWI_{99.9}$  and  $R_{99.9}$  frequency. In CESM1-LE, the mean and upper tails of the individual distributions of  $FWI_{99.9}$  and  $R_{99.9}$  frequency are clearly distinguishable during each study period (see vertical and horizontal probability density plots in Fig. 2, A to C). This suggests that even in cases where the compound event signal in individual grid boxes may be dominated by a particular constituent (e.g., primarily by increases in  $R_{99.9}$  or by increases in  $FWI_{99.9}$ ), both processes are driving changes in compound events on broader spatial scales.

### Role of changes in the seasonality of extreme events

To understand the individual contribution of changes in  $FWI_{99.9}$  and  $R_{99.9}$  to changes in the risk of temporal compounding, we explore the underlying seasonality of changes in  $FWI_{99.9}$  and  $R_{99.9}$  frequency that drive the increases in 3-month, 6-month, and 1-year compounding events in CESM1-LE. In all regions, increases in  $FWI_{99.9}$  events occur during the typical fire weather season (May to September; Fig. 6, A, C, and E). Thus, increases in  $R_{99.9}$  events occurring during and earlier than the typical rainy season shape the

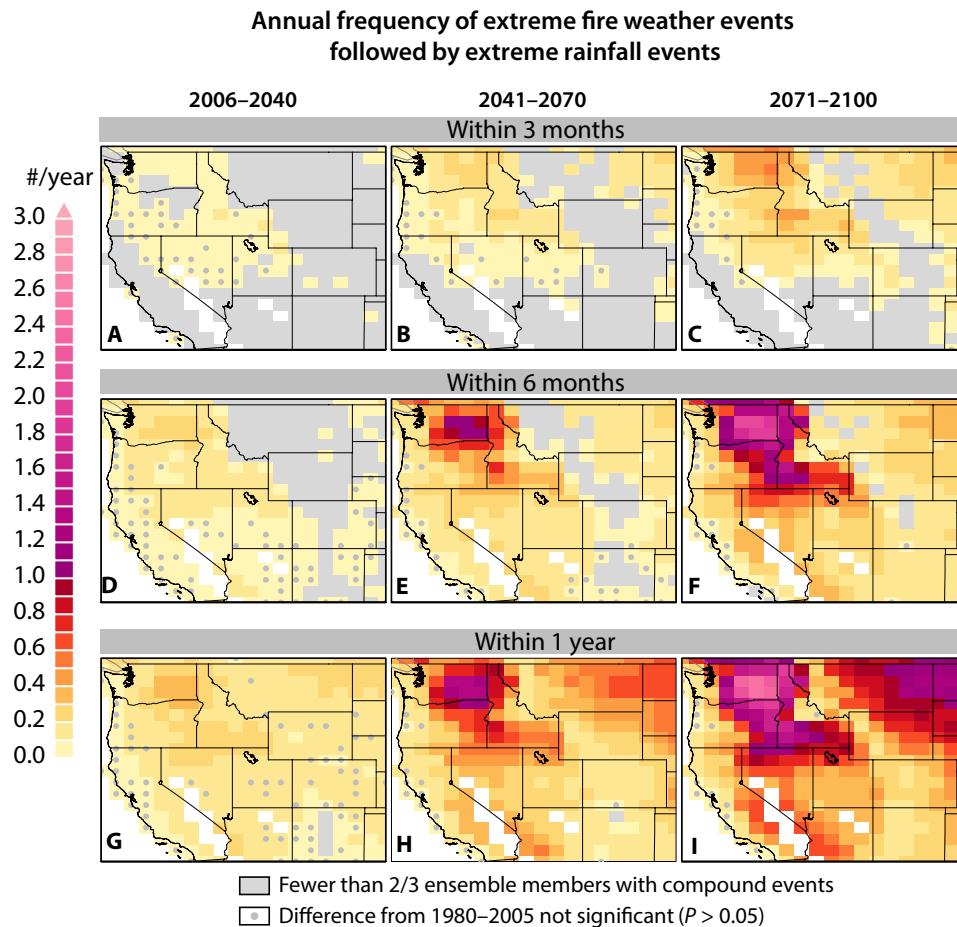


**Fig. 5. Frequency of extreme fire weather events that are followed by extreme rainfall events using CESM1-LE.** The number of compound events per year per grid point that occur within (A to C) 3 months, (D to F) 6 months, and (G to I) 1 year in 2006–2040 (A, D, and G), 2041–2070 (B, E, and H), and 2071–2100 (C, F, and I). Consecutive days that exceed the  $FWI_{99,9}$  threshold are considered as one event, dated on the first consecutive day. Gray areas show where fewer than two-thirds of the ensemble members show at least one compound event occurring. Stippled regions do not have significant ( $P > 0.05$ ) differences in the ensemble distribution of the annual frequency compared to 1980–2005 (shown in fig. S5) calculated using the KS test. White areas are desert, ocean, or surface water. (Results for CanESM2 are shown in fig. S7.)

increases in subannual compounding events in different regions. Increases in  $R_{99,9}$  events in the early fall in PNW and Colorado lead to a rise in 3-month compounding events, with  $\sim 0.25$  more annual events per  $10^5 \text{ km}^2$  in October in Colorado and 2 more in the PNW (Fig. 6, C to F). Large increases in the annual number of 6-month compounding events in 2100 are driven by increases in  $R_{99,9}$  events in the early winter, with up to  $\sim 1$  and  $\sim 4$  more per  $10^5 \text{ km}^2$  in PNW and California, respectively (Fig. 6, A and B). In the spring, increases in  $R_{99,9}$  events largely yield increases in 1-year compounding events, although in Colorado some of these increases in late spring overlap with increases in early summer  $FWI_{99,9}$  events, leading to small increases in 3-month compounding events (Fig. 6). These results provide insight into the subannual timing and seasonality of compounding events, allowing more informed mitigation of potential impacts.

### Temporally compounding events occurring after more than 1 year

While areas burned in a wildfire can start to recover some of their pre-fire conditions after 1 year, post-fire effects on vegetation, soil absorbency, and ground cover can remain up to 8 years after a fire (2). During this time, a burned area will typically experience enhanced

risks of flash floods and debris flows (41). To capture projected risks of such “multiannual” compound events, we quantify changes in  $R_{99,9}$  events occurring within 5 years after an  $FWI_{99,9}$  event.

Among the three regions analyzed in this study, the largest increases in multiannual compound events occur in the PNW in both CESM1-LE and CanESM2. In this region, we find more than a threefold increase in the number of  $FWI_{99,9}$  events that are followed by  $R_{99,9}$  events within 5 years by the end of the 21st century (Fig. 7G), which equates to almost 100% of all extreme fire weather events (Fig. 7H and figs. S6T and S8H). In CESM1-LE, the number of  $R_{99,9}$  events that follow each  $FWI_{99,9}$  event, on average, also triples, to up to 7.5  $R_{99,9}$  events per  $FWI_{99,9}$  event (Fig. 7I). By the end of the 21st century, our findings suggest that almost every  $FWI_{99,9}$  event in PNW will be followed by multiple occurrences of  $R_{99,9}$  events, and very few extreme fire weather events will occur in the absence of a subsequent extreme rainfall event within a 5-year time frame.

Although smaller in magnitude than the very large increases across the PNW, California and Colorado also see statistically significant increases in multiannual compounding events throughout the 21st century in both CESM1-LE and CanESM2. In Colorado, the fraction and number of  $FWI_{99,9}$  events followed by  $R_{99,9}$  events,

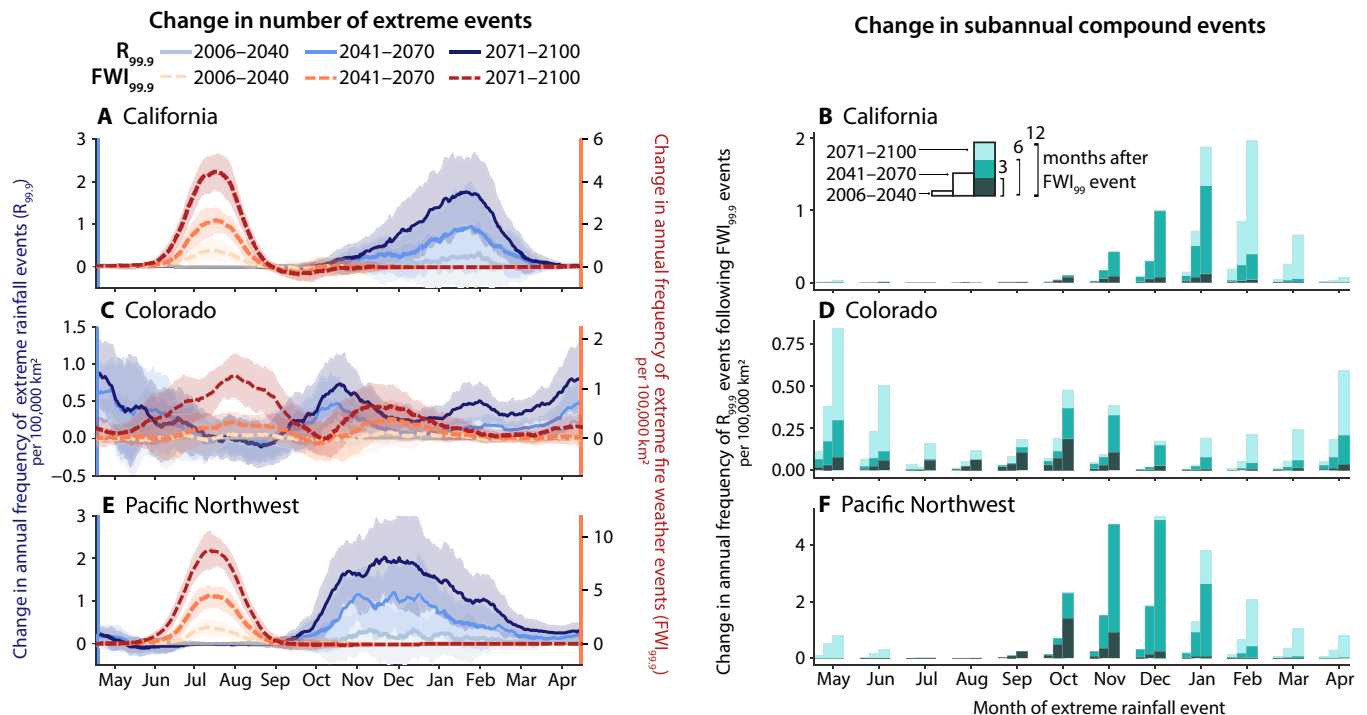


**Fig. 6. Seasonality of changes in extreme rainfall, extreme fire weather, and subannual compounding events using CESM1-LE.** (A, C, and E) Ensemble average change in the annual frequency of extreme rainfall events ( $R_{99.9}$ , left axis, solid blues) and extreme fire weather events ( $FWI_{99.9}$ , right axis, dashed reds) per  $10^5$  km<sup>2</sup> between 1980–2005 and 2006–2040 (light hues), 2041–2070 (medium hues), and 2071–2100 (dark hues) in (A) California, (C) Colorado, and (E) the PNW. A 15-day moving window is used to average values on a given day. (B, D, and F) Ensemble average change in the annual number of  $R_{99.9}$  events that occur 3 months (dark teal), 6 months (light teal), and 12 months (pale turquoise) after an  $FWI_{99.9}$  event for each month per  $10^5$  km<sup>2</sup> in (B) California, (D) Colorado, and (F) the PNW. The bars show the ensemble average of the change in 2006–2040, 2041–2070, and 2071–2100 from left to right, respectively, compared to 1980–2005. The 6-month events are shown as a subset of the 12-month events, and the 3-month events are shown as a subset of the 6-month events. For reference, California is approximately 420,000 km<sup>2</sup>.

and the number of compounding  $R_{99.9}$  events, within 5-year time frames increase substantially until 2070. We note, however, that increases in Colorado weaken throughout the rest of the 21st century in CESM1-LE, whereas the risk of multiannual compounding events continues to increase in California and PNW. Given that the annual frequency of both extreme rainfall and fire weather events continues to increase during this time period in Colorado (Figs. 2B and 3, A and B), this suggests that there may also be changes in the interannual variability of extreme fire weather conditions and extreme rainfall by the end of the 21st century, leading to smaller changes in the risk of multiannual compounding events.

## DISCUSSION

In this analysis, we show that future climate change will substantially amplify the likelihood of temporally compounding extreme fire weather and extreme rainfall events on subannual and multiannual time scales across most of the western United States. Using two single-model large ensemble simulations, we find robust increases in the likelihood and frequency of compounding events across multiple spatial regions (California, PNW, and Colorado) and multiple time scales (both subannual and multiannual events) under the RCP8.5 scenario. In the PNW, these increases are especially notable: Most (~90%) of the future  $FWI_{99.9}$  events will be followed by an  $R_{99.9}$  event within 6 months, and 25% of  $FWI_{99.9}$  events will be followed by an  $R_{99.9}$  event within 3 months. Over a 5-year time frame, almost

all  $FWI_{99.9}$  events will be followed at least one  $R_{99.9}$  event. Not only that, but the number of  $R_{99.9}$  events following  $FWI_{99.9}$  increases, reaching an average of seven spatially colocated  $R_{99.9}$  events per each  $FWI_{99.9}$  event. We also emphasize that both large ensembles analyzed for compound events (CESM1-LE and CanESM2) agree that there will be relatively broad regional increases in the frequency of these temporally compounding events, especially in the PNW. We note that robust and significant increases in the frequency of these compound events emerge in many locations by mid-21st century under RCP8.5, with relatively lower levels of warming compared to the end of century. Therefore, we expect that robust and significant increases in extreme fire weather events followed by extreme rainfall events would also occur under low or intermediate emission pathways (e.g., RCP6.0 or RCP4.5).

This work builds on previous studies, which have projected an increase in the joint annual risk of burned area and extreme precipitation (26), as well as more frequent dry-to-wet year “precipitation whiplash” events in California (25). We make two important distinctions in our study. First, we consider the sequencing of extreme rainfall events occurring after extreme fire weather events, and second, we assess post-fire rainfall compound events on both subannual and multiannual time frames. Similar to (26), we find large increases in compound extreme fire/rainfall events in northern California; however, our analysis also shows robust increases in these compound events over southern California in both CESM1-LE and CanESM2, while (26) does not. This difference could be attributed to the different

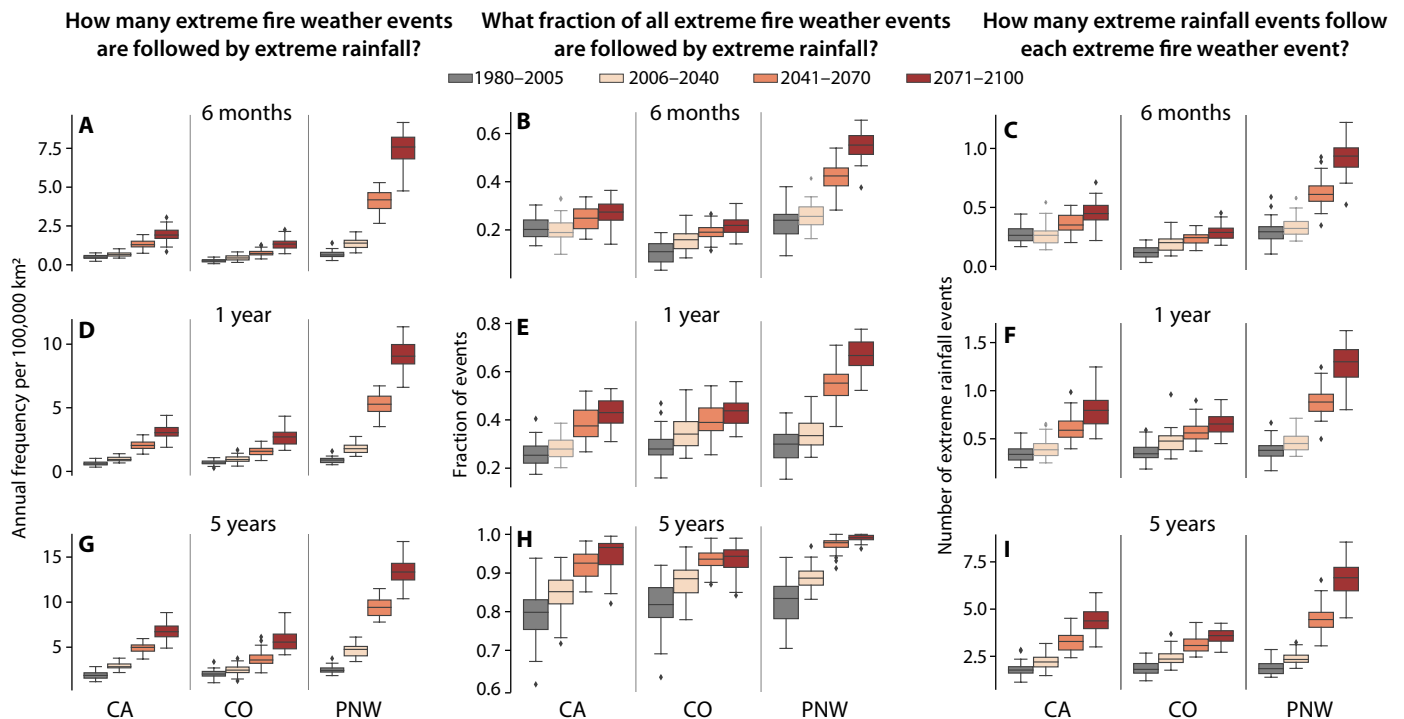


**Fig. 7. How many extreme fire weather events are followed by extreme rainfall using CESM1-LE?** (A, D, and G) Annual frequency per  $10^5$  km<sup>2</sup> of extreme fire weather (FWI<sub>99.9</sub>) events followed by extreme rainfall ( $R_{99.9}$ ) events, (B, E, and H) fraction of FWI<sub>99.9</sub> events followed by  $R_{99.9}$  events, and (C, F, and I) number of  $R_{99.9}$  events that follow FWI<sub>99.9</sub> events within (A to C) 6 months, (D to F) 1 year, and (G to I) 5 years in 1980–2005 (gray), 2006–2040 (peach), 2041–2070 (orange), and 2071–2100 (red) for California, Colorado, and the PNW. The box boundary represents the interquartile range (IQR) across the ensemble, the horizontal line in the box represents the median of the ensemble, and the tails are approximately three times the IQR. The light gray boundaries of boxes show that the ensemble distribution is not significantly different ( $P > 0.01$ ) than the historic period calculated using the KS test.

datasets used [(26) used downscaled data from four general circulation models, each with a single realization] or to the variations in the definitions of the compound event used in each analysis. In addition, by expanding our study domain to encompass the whole western United States, we show that increases in post-fire hydrologic risks in the PNW and Colorado are similar to or more extreme than those in California. In addition, increases in subannual and multi-annual compound events over the PNW at times occur at a faster pace than increases in FWI<sub>99.9</sub> or  $R_{99.9}$  events, individually—suggesting that post-fire hydrologic hazards may increase at an especially rapid rate in a warming climate.

While our study does not investigate the specific dynamical mechanisms behind these changes, there is evidence that observed and projected increases in both extreme fire weather events and extreme rainfall events are largely the product of thermodynamic responses to warming and changes in atmospheric circulation patterns. Increases in temperature and vapor pressure deficit in observations and model simulations have been shown to drive substantial increases in extreme fire weather frequency (12, 20, 42), and increases in extreme rainfall events using global and regional climate model simulations have been strongly linked to increases in atmospheric water vapor, as well as mean circulation changes (24, 25, 37). Changes in the joint occurrence of extreme fire weather and extreme rainfall events on multiannual scales could also be driven by changes in the modes of natural variability [e.g., (25, 37, 43)]. While large ensemble simulations can be used to shed some light on local to regional mechanisms that modify the joint occurrence of these

events, additional sensitivity testing is needed to confirm these processes. Ideally, high-resolution Earth system models with more sophisticated land models would be used to quantify any localized mechanisms in a more detailed and robust way.

Changes in the frequency and severity of wildfire, the size of burned areas, and fire effects on vegetation and hydrology are also important for estimating wildfire impacts and predicting post-fire debris flows and flash floods (2, 6). This study mainly focuses on wildfire-conducive meteorological conditions that are captured with a reasonable degree of accuracy by a coarse-resolution global climate model (CESM1), and therefore does not account for future changes in actual wildfire characteristics including fire frequency and size, fuel (vegetation) conditions, or rates of ignition. Nonetheless, our study shows that extreme fire weather conditions, which are strongly associated with wildfire size and severity [e.g., (11)], are projected to become more prevalent in nearly every portion of the study domain—creating conditions that greatly elevate the risk of wildfires and related post-fire hydrologic hazards.

We acknowledge that our definition of extreme rainfall events may not be suitable to directly assess the risk of debris flows. Relevant rainfall thresholds that could potentially cause these impacts are site and fire specific, leading to the lack of a consistent event-triggering threshold across regions (1, 27). Short-time scale (hourly to sub-hourly) extreme rainfall rates have the largest impact on the risk of debris flows or flash floods across recently burned areas, such as the 15-min 15-mm downpour recorded during the 2018 debris flows in Montecito (3). Short-duration rainfall extremes such as these are



not captured by the daily rainfall amounts used in the present study. This choice was made on the basis of data availability: While daily rainfall data are available over for all models over the full analysis period, subdaily (6 hourly) rainfall data are only available for three short subperiods (1990–2005, 2025–2035, and 2070–2080) for CESM1-LE and may still be too temporally coarse for assessing debris flow or flash flood risks. However, the percentile-based extreme daily rainfall threshold used here nonetheless captures severe wet events that can cause substantial harm to communities (36), induce stress upon water and flood management infrastructure (44), and negatively affect the environment through nutrient transport and soil erosion (45, 46).

Collectively, our findings imply that the risks associated with wildfire-precipitation compound extreme events, including debris flows and flash floods, will likely increase substantially due to climate change across a broad portion of the western United States spanning a wide range of topographical and vegetation regimes. In general, this projected increase stems from an increase in both the frequency of extreme fire and extreme rainfall events—although there is greater uncertainty regarding the relative contribution of fire weather changes in topographically complex regions such as California in the coarser-resolution ensemble (CanESM2). Given the substantial adverse societal impacts of recent post-fire floods and debris flows in California, Colorado, and the PNW, our findings have direct relevance for both short-term emergency management and long-term hazard mitigation and climate adaptation across this region.

## MATERIALS AND METHODS

### Experimental design

We use MMLEA (28) to assess the changes in post-fire hydrologic risks during the historical period (1980–2005) and 21st century (2006–2100) projections, with a focus on the CESM1-LE simulations (29). These single-model initial-condition large ensembles allow us to estimate the anthropogenically forced response of changes in extreme but rare temporally compounding events in the presence of internal climate variability (28, 29). We first quantify the changes in the individual and joint seasonal and annual frequency of extreme fire weather and extreme rainfall events in the 21st century compared to the historic period. We then analyze changes in sequencing of these events to assess post-fire hydrologic risks in future climates.

### Large ensemble climate simulations

We analyze five large ensemble experiments with the available data from MMLEA (28). All models used for these experiments are global with a coupled ocean-land-atmosphere configuration. At the time of analysis, CESM1 (29), CanESM2 (47), CSIRO-Mk3.6 (48), EC-Earth (49), and GFDL-CM3 (50) had daily resolution precipitation data available in their large ensemble experiments, and only CESM1 and CanESM2 included daily resolution variables for calculating FWI (precipitation, maximum temperature, surface wind speed, and relative humidity). The large ensemble experiments of CESM1-LE, CSIRO Mk3-6-0, EC-Earth, and GFDL-CM3 use microinitialization, while CanESM2 uses a combination of micro- and macroinitialization to capture internal variability (28). All large ensemble experiments use the same historical and RCP8.5 forcings and are available over the same analysis period used in the study (1980–2100). We focus our analysis and results on CESM1-LE, given its relatively higher spatial resolution ( $\sim 1.3^\circ \times 0.9^\circ$ ), sufficient data availability

for  $R_{99,9}$  and  $FWI_{99,9}$ , and its relatively large size (40 members). Details of the large ensemble experiments, including the number of ensemble members, resolution, and data availability, are listed in table S1. MMLEA is made available by U.S. CLIVAR Working Group on Large Ensembles at [www.cesm.ucar.edu/projects/community-projects/MMLEA/](http://www.cesm.ucar.edu/projects/community-projects/MMLEA/).

### Extreme fire weather events

When present, wildfire or burned area schemes in the MMLEA simulations differ strongly among the models and can have systemic biases compared to observations (51). For example, the CESM1 model, which does have a parameterized burned area scheme, both systematically overestimates the magnitude of burned area and underestimates the interannual variability of fire emissions in the historic period in the western United States (52, 53). In addition, changes in ignition are not usually accounted for in the fire schemes used in the MMLEA models. This makes the burned area product from any of the MMLEA models unsuitable to quantify the anthropogenic signal in fire activity in both historic and future years. Therefore, we use a modified version of the Canadian Forest FWI (11, 30, 32) to quantify the meteorological conditions that could lead to wildfire ignition and spread on a daily scale, and it allows us to overcome the differences among different land model wildfire schemes. FWI is calculated for CESM1-LE and CanESM2, which are the only two ensembles in MMLEA to have sufficient data for its calculation at the time of analysis. To calculate FWI, we use daily maximum temperature (*tasmax*), precipitation (*pr*), relative humidity (*hurs*), and average surface wind speed (*sfcWind*). *hurs* was not available for CESM1-LE; therefore, it was derived using the MetPy Python package using sea-level pressure (*psl*), lowest water vapor–mixing ratio (*qbot*), and temperature (*tas*) (54). Next, we calculate three fuel moisture codes that reflect the levels of moisture in shallow to deep layers in the soil column using *tasmax*, *pr*, and *hurs*. FWI is then calculated using the three moisture codes and *sfcWind*, and estimates the daily conditions relevant to wildfire occurrence and spread on the daily scale [see (30, 55) for FWI calculation details].

We then identify extreme fire weather days using the grid-level 99.9th percentile of FWI across all the ensemble members for each large ensemble in the historic period (1980–2005) as a threshold [similar to (11–13)]. Consecutive days that exceed this threshold are considered as one extreme fire weather event ( $FWI_{99,9}$ ), dated using the first consecutive day. When using a lower threshold, such as 99th percentile, we found that the spatial and temporal patterns of changes in extreme fire weather frequency are similar to those when using the 99.9th percentile. However, the size of the changes in extreme fire weather frequency are systematically higher for the more extreme percentile, which is an intrinsic product of the underlying statistical distribution, given that rarer events will have larger relative changes (56).

We emphasize that we have used an “atmosphere-only” metric of wildfire risk in this study, i.e., we quantify wildfire risk from a weather perspective and do not explicitly simulate actual fires. Since the actual occurrence of fire is conditionally dependent on ignition, as well as background fuel (vegetation) availability and moisture levels (among other factors), we can only indirectly infer the likelihood that a fire would actually occur. However, prior work has demonstrated that FWI as defined in this study is strongly associated with actual area burned, especially when FWI values are extreme (11), for physical reasons that are likely to hold true even in a nonstationary climate (20). Studies have also shown that the ensemble mean of

CESM1-LE FWI reliably estimates the spatial patterns of the observed FWI in the historic period (12). Thus, we are confident that the occurrence of extreme FWI days is a reasonable proxy for days on which there is high potential for new wildfires to ignite and/or on which existing fires are likely to spread rapidly in the western United States.

### Extreme rainfall events

For CESM1-LE, we first extract nonsnow precipitation from the simulations by subtracting any snow amounts (CESM1 variable names PRECSC and PRESCL) for each day from the total precipitation (PRECT) to calculate daily rainfall amounts. This was done since precipitation events that could lead to flash floods or debris flow are most likely associated with liquid rainfall rather than snow accumulation. Because of the lack of available snow data, we do not do this for other large ensemble simulations and use total daily precipitation (*pr*). We calculate the 99.9th percentile over all the days in the recent historic period (1980–2005) for each grid point across all the ensemble members in each large ensemble to establish the threshold for extreme rainfall events ( $R_{99.9}$ ).

### Defining sub- and multiannual temporally compounding events

For CESM1-LE and CanESM2, we define a temporally compounding event as an  $FWI_{99.9}$  event followed by at least one  $R_{99.9}$  event in the same grid point within a certain time frame (note:  $FWI_{99.9}$  events may be followed by multiple  $R_{99.9}$  events). “Subannual” temporally compounding events are those in which an  $FWI_{99.9}$  event is followed by an  $R_{99.9}$  event within 1 year and are associated with relatively high risk of debris flows and flash floods, significant nutrient transport, and/or straining emergency resources. “Multiannual” compounding events are those in which an  $FWI_{99.9}$  event is followed by an  $R_{99.9}$  event within 2 to 5 years. These events, while likely impactful, are associated with relatively lower risk given the higher potential for the community, economy, and landscape to recover after the  $FWI_{99.9}$  event but before the subsequent  $R_{99.9}$  event (41).

### Statistical analysis

For each large ensemble, we assess changes in the annual and seasonal individual and joint frequency of  $FWI_{99.9}$  and  $R_{99.9}$  events over the 21st century, as well as the changes in temporally compounding events in which an  $R_{99.9}$  follows an  $FWI_{99.9}$  event at the same location. We divide the 21st century into three periods: 2006–2040, 2041–2070, and 2071–2100, and compare them to the historic period (1980–2005). For the maps of changes in the individual frequencies of  $FWI_{99.9}$  and  $R_{99.9}$  events (Fig. 1 and figs. S1 and S3), we show the ensemble mean of changes between the historic and each future period over each grid point. Robust changes are identified when at least two-thirds of the members for each model ensemble agree on the sign of change at each grid point. For the maps of the fraction and number of  $FWI_{99.9}$  events followed by  $R_{99.9}$  events (Figs. 4 and 5 and figs. S5 to S8), we show the ensemble mean for each period. We assess which grid points have at least two-thirds of the ensemble members showing at least one temporally compounding event occurring during that period. In all maps, the changes in the ensemble distributions between the historic period and the three future periods are tested for significance using the Kolmogorov-Smirnov (KS) test.

We also perform regional analyses by area-averaging grid points in California, Colorado, and PNW and normalizing by each region’s

area for each ensemble member (region outlines shown in Fig. 1). In some cases, each member’s regional average is shown (i.e., Fig. 2), and in others, the ensemble mean (or median) is shown along with 1 SD (or interquartile range) of the ensemble distribution (i.e., Figs. 3, 6, and 7 and figs. S2 and S4). In addition, we test for significance of changes in the ensemble distribution of regional averages between the historic and three future periods using the KS test.

### SUPPLEMENTARY MATERIALS

Supplementary material for this article is available at <https://science.org/doi/10.1126/sciadv.abm0320>

### REFERENCES AND NOTES

1. J. W. Kean, D. M. Staley, Forecasting the frequency and magnitude of postfire debris flows across Southern California. *Earths Future* **9**, e2020EF001735 (2021).
2. B. A. Ebel, D. A. Martin, Meta-analysis of field-saturated hydraulic conductivity recovery following wildland fire: Applications for hydrologic model parameterization and resilience assessment. *Hydrol. Process.* **31**, 3682–3696 (2017).
3. N. S. Oakley, F. Cannon, R. Munroe, J. T. Lancaster, D. Gomberg, F. Martin Ralph, Brief communication: Meteorological and climatological conditions associated with the 9 January 2018 post-fire debris flows in Montecito and Carpinteria, California, USA. *Nat. Hazards Earth Syst. Sci.* **18**, 3037–3043 (2018).
4. J. Kershner, Carlton Complex Fire. HistoryLink.org (2014); [www.historylink.org/File/10989](http://www.historylink.org/File/10989).
5. D. M. Staley, E. G. Joseph, J. W. Kean, Objective definition of rainfall intensity-duration thresholds for post-fire flash floods and debris flows in the area burned by the Waldo Canyon fire, Colorado, USA, in *Engineering Geology for Society and Territory—Volume 2: Landslide Processes*, G. Lollino, D. Giordan, G. B. Crosta, J. Corominas, R. Azzam, J. Wasowski, N. Sciarra, Eds. (Springer International Publishing, 2015), vol. 2, pp. 621–624.
6. L. A. Mcguire, N. Oakley, J. W. Kean, D. M. Staley, M. D. E. Orla-barile, Time since burning and rainfall characteristics impact post-fire debris-flow initiation and magnitude. *Environ. Eng. Geosci.* **27**, 43–56 (2021).
7. J. Zscheischler, O. Martius, S. Westra, E. Bevacqua, C. Raymond, R. M. Horton, B. van den Hurk, A. AghaKouchak, A. Jézéquel, M. D. Mahecha, D. Maraun, A. M. Ramos, N. N. Ridder, W. Thiery, E. Vignotto, A typology of compound weather and climate events. *Nat. Rev. Earth Environ.* **1**, 333–347 (2020).
8. C. Raymond, R. M. Horton, J. Zscheischler, O. Martius, A. AghaKouchak, J. Balch, S. G. Bowen, S. J. Camargo, J. Hess, K. Kornhuber, M. Oppenheimer, A. C. Ruane, T. Wahl, K. White, Understanding and managing connected extreme events. *Nat. Clim. Chang.* **10**, 611–621 (2020).
9. J. T. Abatzoglou, A. P. Williams, Impact of anthropogenic climate change on wildfire across western US forests. *Proc. Natl. Acad. Sci. U.S.A.* **113**, 11770–11775 (2016).
10. J. T. Abatzoglou, A. P. Williams, L. Boschetti, M. Zubkova, C. A. Kolden, Global patterns of interannual climate–fire relationships. *Glob. Chang. Biol.* **24**, 5164–5175 (2018).
11. M. Goss, D. L. Swain, J. T. Abatzoglou, A. Sarhadi, C. A. Kolden, A. P. Williams, N. S. Diffenbaugh, Climate change is increasing the likelihood of extreme autumn wildfire conditions across California. *Environ. Res. Lett.* **15**, 094016 (2020).
12. D. Touma, S. Stevenson, F. Lehner, S. Coats, Human-driven greenhouse gas and aerosol emissions cause distinct regional impacts on extreme fire weather. *Nat. Commun.* **12**, 212 (2021).
13. A. P. Williams, J. T. Abatzoglou, A. Gershunov, J. Guzman-Morales, D. A. Bishop, J. K. Balch, D. P. Lettenmaier, Observed impacts of anthropogenic climate change on wildfire in California. *Earths Future* **7**, 892–910 (2019).
14. T. Schoennagel, T. T. Veblen, W. H. Romme, The interaction of fire, fuels, and climate across Rocky Mountain forests. *Bioscience* **54**, 661–676 (2004).
15. E. J. Hanan, J. Ren, C. L. Tague, C. A. Kolden, J. T. Abatzoglou, R. R. Bart, M. C. Kennedy, M. Liu, J. C. Adam, How climate change and fire exclusion drive wildfire regimes at actionable scales. *Environ. Res. Lett.* **16**, 024051 (2021).
16. E. Hjerpe, Y.-S. Kim, L. Dunn, Forest density preferences of homebuyers in the wildland-urban interface. *For. Policy Econ.* **70**, 56–66 (2016).
17. J. Balch, T. Schoennagel, A. P. Williams, J. T. Abatzoglou, M. Cattau, N. Mietkiewicz, L. S. Denis, Switching on the Big Burn of 2017. *Fire* **1**, 17 (2018).
18. D. M. J. S. Bowman, C. A. Kolden, J. T. Abatzoglou, F. H. Johnston, G. R. van der Werf, M. Flannigan, Vegetation fires in the Anthropocene. *Nat. Rev. Earth Environ.* **1**, 500–515 (2020).
19. D. L. Swain, A. Shorter, Sharper rainy season amplifies California wildfire risk. *Geophys. Res. Lett.* **48**, e2021GL092843 (2021).
20. J. T. Abatzoglou, A. P. Williams, R. Barbero, Global emergence of anthropogenic climate change in fire weather indices. *Geophys. Res. Lett.* **46**, 326–336 (2019).

21. D. Singh, M. Tsiang, B. Rajaratnam, N. S. Diffenbaugh, Precipitation extremes over the continental United States in a transient, high-resolution, ensemble climate model experiment. *J. Geophys. Res. Atmos.* **118**, 7063–7086 (2013).
22. D. Rastogi, D. Touma, K. J. Evans, M. Ashfaq, Shift toward intense and widespread precipitation events over the United States by Mid-21st century. *Geophys. Res. Lett.* **47**, 10.1029/2020GL089899 (2020).
23. X. Huang, D. L. Swain, A. D. Hall, Future precipitation increase from very high resolution ensemble downscaling of extreme atmospheric river storms in California. *Sci. Adv.* **6**, eaba1323 (2020).
24. X. Huang, S. Stevenson, A. D. Hall, Future warming and intensification of precipitation extremes: A “double whammy” leading to increasing flood risk in California. *Geophys. Res. Lett.* **47**, e2020GL088679 (2020).
25. D. L. Swain, B. Langenbrunner, J. D. Neelin, A. Hall, Increasing precipitation volatility in twenty-first-century California. *Nat. Clim. Chang.* **8**, 427–433 (2018).
26. H. Moftakhari, A. Aghakouchak, Increasing exposure of energy infrastructure to compound hazards: Cascading wildfires and extreme rainfall. *Environ. Res. Lett.* **14**, (2019).
27. N. S. Oakley, A warming climate adds complexity to post-fire hydrologic hazard planning. *Earths Future* **9**, e2021EF002149 (2021).
28. C. Deser, F. Lehner, K. B. Rodgers, T. Ault, T. L. Delworth, P. N. DiNezio, A. Fiore, C. Frankignoul, J. C. Fyfe, D. E. Horton, J. E. Kay, R. Knutti, N. S. Lovenduski, J. Marotzke, K. A. McKinnon, S. Minobe, J. Rinderson, J. A. Screen, I. R. Simpson, M. Ting, Insights from Earth system model initial-condition large ensembles and future prospects. *Nat. Clim. Chang.* **10**, 277–286 (2020).
29. J. E. Kay, C. Deser, A. Phillips, A. Mai, C. Hannay, G. Strand, J. M. Arblaster, S. C. Bates, G. Danabasoglu, J. Edwards, M. Holland, P. Kushner, J.-F. Lamarque, D. Lawrence, K. Lindsay, A. Middleton, E. Munoz, R. Neale, K. Oleson, L. Polvani, M. Verstein, The Community Earth System Model (CESM) large ensemble project: A community resource for studying climate change in the presence of internal climate variability. *Bull. Am. Meteorol. Soc.* **96**, 1333–1349 (2015).
30. C. E. Van Wagner, *Structure of the Canadian Forest Fire Weather Index*, (Canadian Forest Service Publications, 1974).
31. F. Batista, “Amazon rainforest fire season starts with outlook for record burn,” *Bloomberg Green*, 2020; [www.bloomberg.com/news/articles/2020-06-08/the-amazon-is-still-burning-only-now-the-world-isn-t-watching](http://www.bloomberg.com/news/articles/2020-06-08/the-amazon-is-still-burning-only-now-the-world-isn-t-watching).
32. B. M. Wotton, Interpreting and using outputs from the Canadian Forest Fire Danger Rating System in research applications. *Environ. Ecol. Stat.* **16**, 107–131 (2009).
33. R. Barbero, J. T. Abatzoglou, E. A. Steel, N. K. Larkin, Modeling very large-fire occurrences over the continental United States from weather and climate forcing. *Environ. Res. Lett.* **9**, 124009 (2014).
34. N. Maher, S. B. Power, J. Marotzke, More accurate quantification of model-to-model agreement in externally forced climatic responses over the coming century. *Nat. Commun.* **12**, 788 (2021).
35. J. T. Abatzoglou, B. J. Hatchett, P. Fox-Hughes, A. Gershunov, N. J. Nauslar, Global climatology of synoptically-forced downslope winds. *Int. J. Climatol.* **41**, 31–50 (2021).
36. L. M. Bouwer, Projections of future extreme weather losses under changes in climate and exposure. *Risk Anal.* **33**, 915–930 (2013).
37. X. Huang, S. Stevenson, Connections between mean North Pacific circulation and Western US precipitation extremes in a warming climate. *Earths Future* **9**, e2020EF001944 (2021).
38. S. Pfahl, P. A. O’Gorman, E. M. Fischer, Understanding the regional pattern of projected future changes in extreme precipitation. *Nat. Clim. Chang.* **7**, 423–427 (2017).
39. X. Huang, D. L. Swain, D. B. Walton, S. Stevenson, A. D. Hall, Simulating and evaluating atmospheric river-induced precipitation extremes along the U.S. Pacific coast: Case studies from 1980–2017. *J. Geophys. Res. Atmos.* **125**, e2019JD031554 (2020).
40. G. Zappa, Regional climate impacts of future changes in the mid-latitude atmospheric circulation: A storyline view. *Curr. Climate Change Rep.* **5**, 358–371 (2019).
41. B. A. Ebel, Temporal evolution of measured and simulated infiltration following wildfire in the Colorado Front Range, USA: Shifting thresholds of runoff generation and hydrologic hazards. *J. Hydrol.* **585**, 124765 (2020).
42. Y. Zhuang, R. Fu, B. D. Santer, R. E. Dickinson, A. Hall, Quantifying contributions of natural variability and anthropogenic forcings on increased fire weather risk over the western United States. *Proc. Natl. Acad. Sci. U.S.A.* **118**, e2111875118 (2021).
43. A. G. Pendergrass, R. Knutti, F. Lehner, C. Deser, B. M. Sanderson, Precipitation variability increases in a warmer climate. *Sci. Rep.* **7**, 17966 (2017).
44. C. C. Rhoades, D. Entwistle, D. Butler, The influence of wildfire extent and severity on streamwater chemistry, sediment and temperature following the Hayman Fire, Colorado. *Int. J. Wildl. Fire* **20**, 430–442 (2011).
45. A. J. Rust, T. S. Hogue, S. Saxe, J. McCray, Post-fire water-quality response in the western United States. *Int. J. Wildl. Fire* **27**, 203–216 (2018).
46. L. F. Debano, The role of fire and soil heating on water repellency in wildland environments: A review. *J. Hydrol.* **231–232**, 195–206 (2000).
47. M. C. Kirchmeier-Young, F. W. Zwiers, N. P. Gillett, A. J. Cannon, Attributing extreme fire risk in Western Canada to human emissions. *Clim. Change* **144**, 365–379 (2017).
48. S. Jeffrey, L. Rotstayn, M. Collier, S. Dravitzki, C. Hamalainen, C. Moeseneder, K. Wong, J. Syktus, Australia’s CMIP5 submission using the CSIRO-Mk3.6 model. *Aust. Meteorol. Oceanogr. J.* **63**, 1–13 (2013).
49. W. Hazeleger, C. Severijns, T. Semmler, S. Ştefănescu, S. Yang, X. Wang, K. Wyser, E. Dutra, J. M. Baldasano, R. Bintanja, P. Bougeault, R. Caballero, A. M. L. Ekman, J. H. Christensen, B. Van Den Hurk, P. Jimenez, C. Jones, P. Källberg, T. Koening, R. McGrath, P. Miranda, T. Van Noije, T. Palmer, J. A. Parodi, T. Schmith, F. Selten, T. Storelvmo, A. Sterl, H. Tapamo, M. Vancoppenolle, P. Viterbo, U. Willén, EC-Earth: A seamless Earth-system prediction approach in action. *Bull. Am. Meteorol. Soc.* **91**, 1357–1363 (2010).
50. L. Sun, M. Alexander, C. Deser, Evolution of the global coupled climate response to Arctic sea ice loss during 1990–2090 and its contribution to climate change. *J. Climate* **31**, 7823–7843 (2018).
51. S. S. Rabin, J. R. Melton, G. Lasslop, D. Bachelet, M. Forrest, S. Hantson, J. O. Kaplan, F. Li, S. Mangeon, D. S. Ward, C. Yue, V. K. Arora, T. Hickler, S. Kloster, W. Knorr, L. Nieradzki, A. Spessa, G. A. Folberth, T. Sheehan, A. Voulgarakis, D. I. Kelley, I. Colin Prentice, S. Sitch, S. Harrison, A. Arnett, The Fire Modeling Intercomparison Project (FireMIP), phase 1: Experimental and analytical protocols with detailed model descriptions. *Geosci. Model Dev.* **10**, 1175–1197 (2017).
52. S. Kloster, G. Lasslop, Historical and future fire occurrence (1850 to 2100) simulated in CMIP5 Earth System Models. *Glob. Planet. Change* **150**, 58–69 (2017).
53. D. S. Ward, E. Shevliakova, S. Malyshev, J. F. Lamarque, A. T. Wittenberg, Variability of fire emissions on interannual to multi-decadal timescales in two Earth system models. *Environ. Res. Lett.* **11**, 125008 (2016).
54. R. M. May, S. C. Arms, P. Marsh, E. Bruning, J. R. Leeman, K. Goebbert, J. E. Thielen, Z. S. Bruick, MetPy: A [Python] package for meteorological data (2021); 10.5065/D6WW7G29.
55. A. J. Dowdy, G. A. Mills, K. Finkele, W. De Groot, Australian fire weather as represented by the McArthur Forest Fire Danger Index and the Canadian Fire Weather Index and the Australian fire weather as represented by the McArthur Forest Fire Danger Index and the Canadian Fire Weather Index (2009); <http://citesseerx.ist.psu.edu/viewdoc/download?doi=10.1.1.307.8282&rep=rep1&type=pdf>.
56. D. L. Swain, O. E. J. Wing, P. D. Bates, J. M. Done, K. A. Johnson, D. R. Cameron, Increased flood exposure due to climate change and population growth in the United States. *Earths Future* **8**, e2020EF001778 (2020).

#### Acknowledgments

**Funding:** This work was funded by the following: Joint collaboration between the Institute of the Environment and Sustainability at the University of California, Los Angeles, the Center for Climate and Weather Extremes at the National Center for Atmospheric Research, the Nature Conservancy of California, and National Science Foundation grant number 1854761 (to D.L.S.); U.S. Department of Energy grant DE-SC0019418 (to S.S. and X.H.); and Startup grant provided to D.S. by Washington State University Vancouver (to D.A.K.). **Author contributions:** Conceptualization: D.T., S.S., D.L.S., and D.S. Methodology: D.T., S.S., D.L.S., D.S., D.A.K., and X.H. Formal analysis, investigation, and visualization: D.T. Writing—original draft: D.T. Writing—review and editing: D.T., S.S., D.L.S., D.S., D.A.K., and X.H. **Competing interests:** The authors declare that they have no competing interests. **Data and materials availability:** All data needed to evaluate the conclusions in the paper are present in the paper and/or the Supplementary Materials. Data used to make the main and supplementary figures can be found at [https://github.com/detouma/Touma\\_2022\\_SciAdv](https://github.com/detouma/Touma_2022_SciAdv).

Submitted 23 August 2021

Accepted 10 February 2022

Published 1 April 2022

10.1126/sciadv.abm0320

## Climate change increases risk of extreme rainfall following wildfire in the western United States

Danielle ToumaSamantha StevensonDaniel L. SwainDeepti SinghDmitri A. KalashnikovXingying Huang

*Sci. Adv.*, 8 (13), eabm0320. • DOI: 10.1126/sciadv.abm0320

### View the article online

<https://www.science.org/doi/10.1126/sciadv.abm0320>

### Permissions

<https://www.science.org/help/reprints-and-permissions>

Use of this article is subject to the [Terms of service](#)

---

*Science Advances* (ISSN ) is published by the American Association for the Advancement of Science. 1200 New York Avenue NW, Washington, DC 20005. The title *Science Advances* is a registered trademark of AAAS.  
Copyright © 2022 The Authors, some rights reserved; exclusive licensee American Association for the Advancement of Science. No claim to original U.S. Government Works. Distributed under a Creative Commons Attribution NonCommercial License 4.0 (CC BY-NC).